ELSEVIER

Polymer 41 (2000) 6597–6602

polymer

Plastic deformation in polypropylene/(ethylene–propylene) copolymer blend during paint debonding

E. Tomasetti[a,b], R. Legras[a], B. Henri-Mazeaud[c], B. Nysten[a,*]

[a]*Unité de chimie et de physique des hauts polymères, Université catholique de Louvain, place Croix du sud, 1, B-1348 Louvain-la-Neuve, Belgium*
[b]*Unité de chimie des interfaces, Université catholique de Louvain, place Croix du sud, 1, B-1348 Louvain-la-Neuve, Belgium*
[c]*Direction de la Recherche, Renault, rue des Bons-Raisins, 67, F-92500 Reuil-Malmaison, France*

Received 10 December 1998; received in revised form 5 November 1999; accepted 8 December 1999

Abstract

Polypropylene (PP) and polypropylene/(ethylene–propylene) copolymer (EP) blend (PP/EP) injection-moulded plates were painted with a chlorinated polypropylene (CPO) based adhesion promoter. Three-point bending and crosscut adhesion tests performed on these plates show that adherence is better on PP/EP than on PP. X-ray photoelectron spectroscopy (XPS) and force modulation microscopy (FMM) analyses were performed on the failure surface obtained after the three-point bending test. XPS shows that the Cl atomic fraction is less than 0.5% on the polymer side and close to 4% on the paint side indicating that the fracture is located at the CPO–polymer interface. The analysis of the PPEP surface by FMM reveals that paint debonding occurs with plastic deformations located into the EP elastomer phase. The magnitude of the plastic deformation is dependent on the depth location of the nodules. The adherence improvement induced by the presence of EP nodules can thus be explained by energy dissipation occurring during EP deformation.

Keywords: Polypropylene; Adhesion; Surface analysis

1. Introduction

The amount of polypropylene/ethylene–propylene copolymer blends (PP/EP) used in the automotive industry is increasing spectacularly. It is used for bumpers, fascia, dashboard and others parts of the car body. Exterior automotive components are painted to increase the lifetime of the part and to enhance the aesthetic appearance. However, PP/EP has a low surface energy preventing paint adhesion on the surface [1]. The introduction of EP in PP improves paint adhesion but this is not sufficient [2–5] and an adhesion promoter is required. A common method generally consists in applying a thin chlorinated polypropylene layer (CPO) [3,6]. The adhesion improvement due to the presence of EP in the substrate and the use of CPO as adhesion promoter are not well understood. It is generally inferred that CPO molecules could diffuse in EP and improve adhesion by molecular entanglement [1,3–5,7,8]. Indeed, CPO diffusion was recently demonstrated [9] and shown to be forced by the solvent, which swells the polymer substrate. The low crystallinity of EP facilitates this process. However, some authors [3,4] reported that EP addition into PP improved adhesion even without adhesion promoter. Viscoelastic and plastic deformations consuming energy during failure could explain this improvement. As a matter of fact, this phenomenon is expected to be predominant in the elastomeric phase [10,11] and to depend on the surface morphology.

In previous studies [12,13], it was shown that the mapping by atomic force microscopy (AFM) and by force modulation microscopy (FMM) of the elastic properties of injection-moulded PP/EP plates reveals without any pretreatment the surface morphology (EP nodules dispersion). A quantitative analysis of the elastic modulus revealed that EP nodules appear stiffer at the surface than in the bulk. This effect was attributed to the presence of a thin PP layer covering the nodules.

The aim of this paper is to get a better understanding on the role of EP in the deformation mechanism involved during paint debonding. In order to achieve this goal, adhesion tests were performed on PP and PP/EP painted plates. Failure surfaces were then carefully characterised by X-ray photoelectron spectroscopy (XPS), transmission electron microscopy (TEM) and FMM.

* Corresponding author. Fax: + 32-010-451593.
E-mail address: nysten@poly.ucl.ac.be (B. Nysten).

0032-3861/00/$ - see front matter
PII: S0032-3861(99)00885-X

Table 1
Characteristics of the polymers used in the present study: Young's modulus, *E*, and Melt Flow Index (MFI) measured at 230°C under 21.6 N

Polymer	*E* (MPa)	MFI (g min^{-1})
PP	1500	25
PP/EP	950	8

2. Experimental

2.1. Materials

Polymers used were PP (Moplen z305) and PP/EP reactor-blends (Hifax SP179, 23% EP) supplied by Montell (Ferrara, Italy). The properties of these polymers are given in Table 1. Both polymers are hydrophobic and present similar contact angle to water. Plates of $100 \times 150 \times 3\ mm^3$ were injection-moulded with a DK300T Codim injection press (screw diameter 42 mm) by Renault (Rueil-Malmaison, France) under the following conditions: material temperature 260°C, mould temperature 35°C, screw displacement speed 42 mm/s.

Paints were supplied by PPG (Saultain, France). The plates were painted by Renault according to the following procedure: surface degreasing with iso-propanol; spray application of the CPO 343-1 based adhesion promoter (Y072I400); application of the base coat (R727A403, "bleu Egée 454", ≅12–18 μm-thick) in two successive spraying steps (2 min delay between steps); spray application after 10 min of the two-components varnish (resin R5500I401, hardener R599I401, ≅35∼40 μm-thick) in two steps; after 10 min, baking at 80°C during 30 min.

2.2. Adhesion tests

Crosscut test was carried out according to test method 1254 of Renault. Four horizontal and four vertical cuts were made in the coating with a knife respecting a distance of 1 mm between parallel cuts. Approximately 20 crosscut-test areas were made per plate. The crosscut areas were covered with an adhesive tape (3M, ref. 250) that was then manually removed. The crosscut area was then visually inspected and evaluated. The adherence level was estimated as follows: 4 when no coating square was removed (excellent adhesion), 3 when less than 50% of squares were removed, 2 when more than 50% of squares were

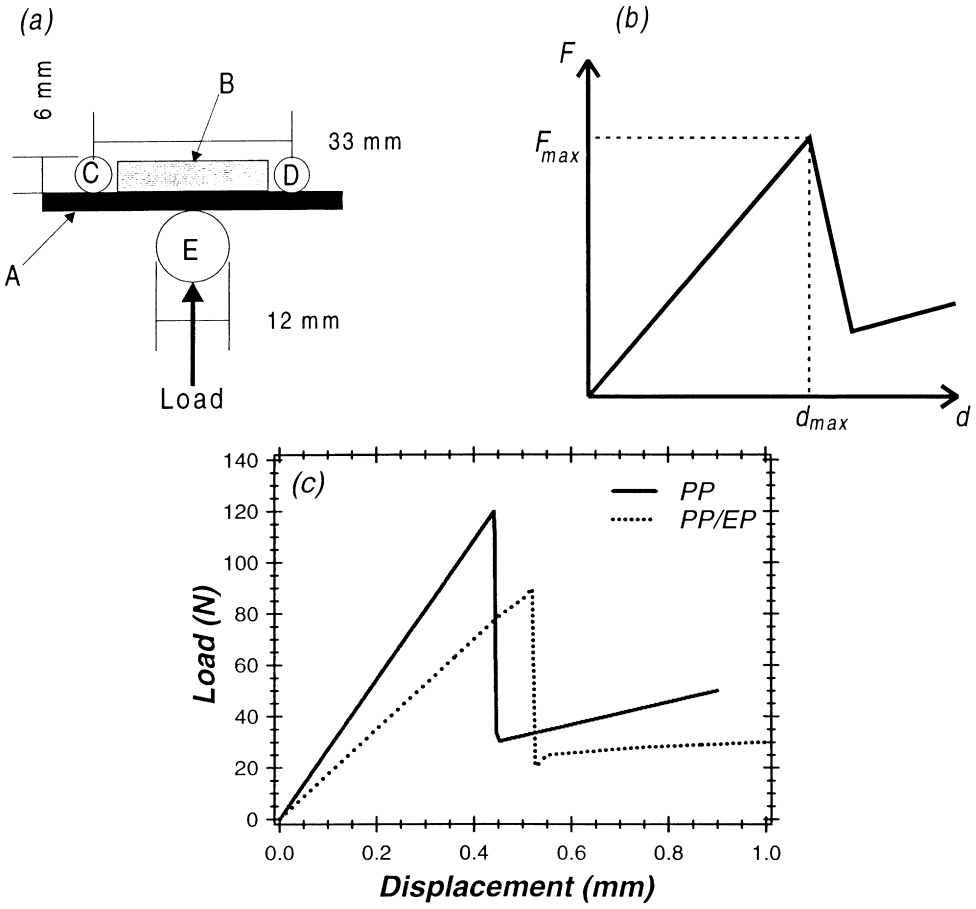

Fig. 1. (a) Schematic diagram of the three-point bending test: sample A; stiffening block B and supports C,D,E. The external supports, C and D, are fixed and the load is applied on the central support E. (b) Schematic representation of a typical force–displacement curve. (c) Typical *F–d* curves, respectively, measured on PP (solid curve) and on PP/EP (dotted curve).

removed, 1 when that almost all coating squares were removed (poor adhesion). For both PP and PP/EP polymers, three plates were tested.

For the three-point bending test (Fig. 1), a stiffening rectangular block is glued in the middle of the coated side of test plates ($3 \times 10 \times 50\ mm^3$). The sample is placed between three supports and then loaded as shown in Fig. 1(a). During the test, the load and the support displacement are recorded to give a force vs. displacement curve ($F–d$ curve) as shown in Fig. 1(b). The slope of the force–displacement curve ($F–d$ slope) is a function of the system rigidity. The paint debonds when a critical force–displacement couple (F_{max},d_{max}) is reached. Coating delamination starts at one of the outer edges of the stiffening block and the crack propagates. In this work, a bi-component epoxy resin (3M, scotch weld 3525B/A) was used as stiffening block. In order to ensure good adhesion between the coating and the stiffening block, the painted side was slightly roughened with an abrasive and then cleaned with isopropanol. The cleaned sample was placed in a holding system containing a silicone mould with a cavity ($25 \times 5 \times 5\ mm^3$) in which the epoxy resin was poured and cured at 65°C during 2 days. All samples were stored for 1 week in ambient conditions before being tested. Tests were carried out on a three-point bending apparatus (Flex 3) supplied by Techlab (Lyon, France) with a displacement speed of $0.5\ mm\ min^{-1}$. For each material, six samples originating from two plates were tested.

2.3. Analytical methods

XPS analyses were performed with a SSI X-Probe (SSX-100/206) photoelectron spectrometer from Fisons. The general principle of the XPS analysis used are described in detail elsewhere [14,15]. Survey spectrum and C_{1s}, O_{1s}, N_{1s}, Si_{2p} spectra were recorded in this order. The binding energies were determined by reference to the C_{1s} component due to C–C and C–H bonds, set at 284.8 eV. The peak intensity was determined by measuring the area after background subtraction using Shirley method [16]. The atomic concentration ratio was calculated on the basis of the acquisition parameters and the sensitivity factors given by the manufacturer. All measurements were duplicated.

In AFM, the sample is mounted on a piezoelectric translator and placed in contact with a sharp tip mounted on a soft cantilever. The cantilever deflexion proportional to the tip–sample interaction force is measured by detecting the angular deflexion of a laser beam reflected from the back of the cantilever extremity [17]. While the sample is scanned horizontally below the tip, the tip–sample interaction force is kept constant by a feedback loop that moves the sample up and down as the tip follows the surface contours. A 3D topographic image of the sample surface is thus obtained by plotting the sample vertical motion as a function of its lateral position. In FMM, a modulation of the sample vertical position is added to its contact equilibrium position and the subsequent modulation movement of the cantilever deflexion is measured by means of a lock-in amplifier [18,19]. The amplitude of the cantilever response is influenced by the elastic properties of the surface: the higher the response amplitude, the higher the surface stiffness.

AFM and FMM images were recorded in air with an Autoprobe CP from Park Scientific Instruments (Sunnyvale, CA) using a 100-μm scanner. The cantilevers were 2 μm-thick silicon Ultralevers® (Park Scientific Instruments) with stiffness, k_c, typically equal to $20\ N\ m^{-1}$. Topographic AFM and elastic FMM images were simultaneously recorded with a scanning frequency equal to $0.4\ lines\ s^{-1}$ and using a contact force ranging between 10 and 200 nN. For force modulation, the sample vertical position was modulated by adding a sinusoidal signal to the z-voltage applied to the piezoelectric scanner. The modulation amplitude, z_1, was equal to 7 Å and the frequency was equal to 2 kHz. The deflexion signal of the cantilever, d_1, was measured with a dual phase lock-in amplifier (EG&G Princeton Applied Research, Model 5210). The local surface elastic modulus was also evaluated by measuring at certain points, the system elastic response, i.e. the ratio between the sample modulation amplitude and the amplitude of the cantilever response, d_1/z_1, which is proportional to the local stiffness [12].

TEM pictures were obtained with a TEM EM301 Philips microscope (80 kV). Sections of 80 nm thickness were obtained by cutting samples at −100°C with a glass knife at −40°C using a Reichert Ultracuts FCS microtome.

Table 2
Results of the adherence tests (three-point bending and crosscut)

	Three-point bending			Cross-cut
	$F–d$ slope (N/mm)	F_{max} (N)	d_{max} (mm)	
PP	288 ± 9	110 ± 8	0.40 ± 0.04	1
PP/EP	175 ± 5	90 ± 5	0.52 ± 0.05	2–3

3. Results

3.1. Adhesion tests

Typical three-point bending curves, respectively, measured on PP and on PP/EP are given in Fig. 1(c). The results of the three-point bending and crosscut tests performed on PP and PP/EP painted plates are given in Table 2. In three-point bending, $F–d$ slope and F_{max} is higher for PP than for PP/EP while d_{max} is lower. According to the crosscut test, PP/EP has a better adherence than PP.

3.2. XPS analysis

The failure surfaces resulting from the three-point bending tests were analysed by XPS. Table 3 gives the surface composition obtained for unpainted surfaces and for failure surfaces of PP/EP and PP plates. For both PP and PP/EP failure surfaces, the Cl atomic fraction is lower

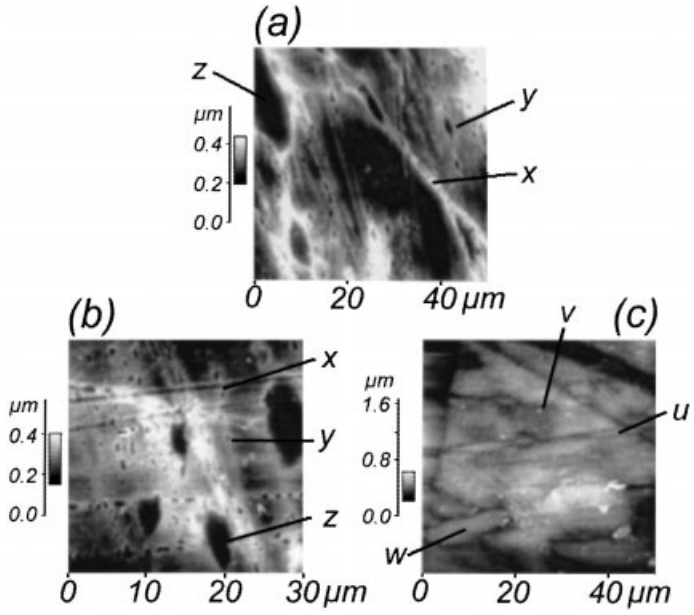

Fig. 2. AFM topographic images recorded on PP surfaces: (a) unpainted plate; (b) substrate side and (c) paint side of a painted plate. x: groove, y: small hole, z: large hole, u: protruding line, v: small bump, w: large bump.

than 0.5% on the substrate side and close to 4% on the paint side. It must be pointed out that high concentrations of Si and O are found on failure surfaces. It is due to the use of silicone mould for the sample preparation for the three-point bending test. In fact, the silicone mould has probably contaminated the surfaces of the stiffening block and of the sample. Consequently, during the sample storage after the adhesion test and before surface analysis, silicone may have migrated to the failure surface.

3.3. AFM and FMM analyses

The AFM and FMM characterisation of unpainted surfaces have been carried out for both PP and PP/EP. Fig. 2(a) presents the topographic image obtained on a PP plate and Fig. 3(a) and (d) the topographic and the elastic images recorded on a PP/EP plate. The PP surface presents grooves, a few large holes (width ≅10 μm) and several small holes (width ≤1 μm). The topography of the PP/EP

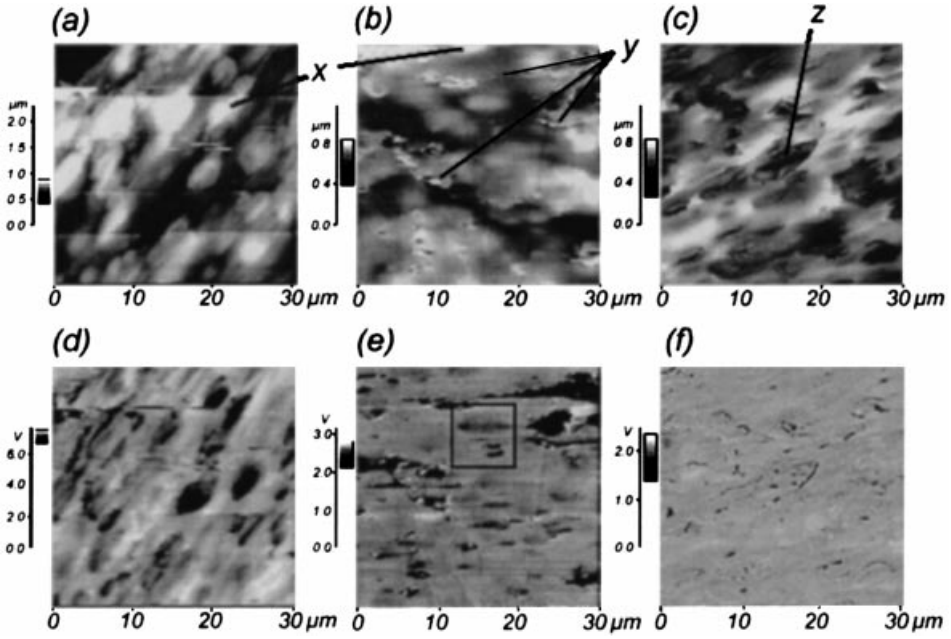

Fig. 3. (a),(b),(c) AFM topographic and (d),(e),(f) FMM elastic images of PP/EP surfaces. (a) and (d) unpainted plate, (b) and (e) substrate side and (c) and (f) paint side of failure surfaces. x: bump, y: tears and z: large hole.

Table 3
Atomic concentration of elements measured by XPS on unpainted surfaces and on failure surfaces (substrate and paint sides)

Element	PP/EP		PP		Unpainted surfaces
	Substrate side	Paint side	Substrate side	Paint side	
C	73.0	72.2	88.0	73.4	99.0
Cl	0.2	4.3	0.4	4.0	0.0
O	16.4	14.0	7.4	15.3	1.0
Si	10.4	9.5	4.2	7.3	0.0

plate (Fig. 3(a)) shows black and white zones. The white zones are composed of few bumps (width ≅ 3–8 μm). On FMM images, bright regions correspond to stiffer material and dark ones to softer material. In Fig. 3(d), soft regions (EP nodules) embedded in the rigid PP could be observed on the surface of the unpainted PP/EP plates.

The topographic images recorded on the substrate side and on the paint side of failure surfaces of PP plates are presented in Fig. 2(b) and (c). The same morphology is found on the substrate side of the failure surface than on the PP unpainted surface (Fig. 2(a)). Conversely, the paint side of the failure surface (Fig. 2(c)) is composed of protruding lines, large and small bumps; it thus appears to be a negative replica of the substrate morphology.

In Fig. 3, topographic and corresponding elastic images taken on a substrate side (b) and (e) and paint side (c) and (f) of failure surfaces from painted PP/EP are presented. The morphology observed on the unpainted plate (Fig. 3(a)) is also observable on the substrate side. Conversely, holes with similar dimensions are observed on the paint side. Moreover, on the substrate side, local deformations like tears consecutive to paint debonding can be observed. On the FMM image of the substrate side (Fig. 3(e)), darker EP nodules are observed as on the unpainted surface. Conversely, no elastic contrast is observed on the paint side of the failure surface. In fact, in this image, only narrow black lines corresponding to noise induced by coarse topographic variations are observed. Thus, the elastic response on this surface is homogeneous and globally corresponds to stiff material. A comparison between topographic and corresponding elastic images taken on the substrate side of the failure surface (Fig. 3(b) and (e)) reveals that topographic deformations (tears) always correspond to darker zones, i.e. EP nodules. More detailed images were obtained by reducing the scanning size. Fig. 4(a) and (b) shows topographic and elastic images recorded in the square delimited in Fig. 3(e). In Fig. 4(b), four EP nodules are noted A, B, C and D. The corresponding topographic image shows that only nodules A and B have undergone plastic deformations during paint debonding as revealed by tears. Local force modulation measurements were carried out on the four nodules. The measured d_1/z_1 ratios proportional to the local stiffness are given in Table 4. The A and B nodules present lower ratios than the C and D nodules. This means that they are apparently softer or, more precisely that they are located closer to the surface. Indeed, previous studies [12] have shown that the elastic response, d_1/z_1, is related to the depth location of EP nodules in PP/EP blends.

Table 4
Local force modulation elastic responses measured on nodules of the four nodules of Fig. 4(b)

Nodule	d_1/z_1 [a]
A	0.40 ± 0.02
B	0.41 ± 0.03
C	0.52 ± 0.02
D	0.47 ± 0.01

[a] Mean values and standard deviations on five measurements.

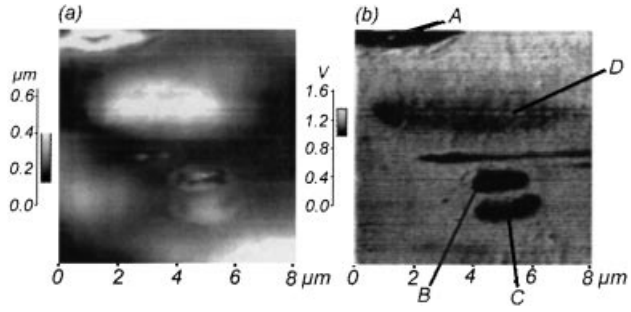

Fig. 4. Detailed topographic (a) and elastic (b) images of the substrate side of PP/EP failure surface corresponding to the square in Fig. 3(e).

Fig. 5 presents a TEM picture performed on cross-section perpendicular to the surface of a PP/EP painted plate. From the top to the bottom of the picture, three successive layers are observed: the base coat, the CPO layer and the PP/EP substrate, with darker EP nodules in the light-grey PP matrix. Paint debonding occurred during sample sectioning at the CPO–substrate interface. Plastic deformation of an EP nodule located very close to the surface could be clearly observed.

4. Discussion

The study using the three-point bending test of several systems with varying rigidity shows that F_{max} is correlated with the F–d slope and thus with the system rigidity which is not the case for d_{max}. The dependence of F_{max} on the rigidity was already mentioned in the literature [20]. Thus the higher rigidity of PP compared to PP/EP can explain the higher F_{max} obtained on PP. Conversely, the performed measurements show that d_{max} is less dependent on the system rigidity. So when samples differ by their rigidity, like PP and PP/EP, the best criterion to characterise their adherence levels becomes d_{max} rather than F_{max}. Higher d_{max} for PP/EP indicates that the adherence is better on PP/EP than on PP. This is confirmed by the better behaviour of PP/EP in the crosscut test (Table 2) compared to PP.

XPS analyses systematically show a higher concentration of chlorine, coming from CPO, on the paint side of failure surfaces than on the substrate side (Table 3). On the other

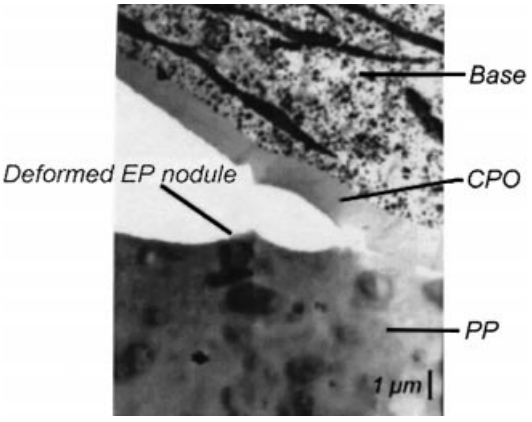

Fig. 5. TEM picture of a cross-section perpendicular to the surface of a painted PP/EP plate. From top to bottom, the successive layers are the base coat, the CPO layer and the PP/EP substrate with darker EP.

hand, nitrogen, present in paint, is absent on both sides. This indicates that the failure is located at the substrate–CPO interface and that this interface is rather sharp. This sharp interface is also observed on TEM images. The low Cl concentration detected on the substrate side could be explained either by CPO diffusion into the substrate or by CPO trapping on surface depressions.

The topographic AFM images obtained on PP plates (Fig. 2) show that the morphology of the substrate side of failure surfaces is very similar to that of unpainted surfaces, while the morphology of the paint side is a negative replica of the substrate morphology. The AFM results thus confirm that the failure is located at the CPO–PP interface. Moreover, it appears that, on PP, paint debonding occurs without noticeable plastic deformation corresponding to a rather brittle failure.

For PP/EP plates, the general morphological aspect of the unpainted surface is globally preserved on the substrate side of the failure surfaces. EP nodules are observed at the surface of both types of surfaces but not on the paint side of failure surfaces. The failure thus also appears to be located at the CPO–PP/EP interface. However, plastic deformations are observed on the substrate side after paint debonding specifically in EP nodules. These deformations require energy and leads to rather ductile failures. This result could explain the adherence improvement due the introduction of EP into PP through the introduction of plastic deformations consuming energy during adhesion failure. The comparison between topographic and elastic images of the substrate side in Fig. 4 reveals that all the EP nodules are not deformed to the same extent. Local force modulation measurements (Table 4) indicate that the EP nodules that have undergone the largest deformation are the softest ones. In a previous study [13], it was shown that surface EP nodules are covered by a thin PP surface layer. The apparent surface stiffness measured on EP nodules was related to their depth location below the surface: nodules closer to the surface appear softer. Consequently, the intensity of the plastic deformation of the EP nodules appears to be related to their depth location; nodules closer to the surface are more deformed. The TEM picture in Fig. 5 also shows interfacial failure with plastic deformation located in EP nodules located closer to the surface. This picture illustrates and confirms the interpretation of the AFM and FMM images of the failure surfaces.

5. Conclusions

Adhesion tests performed in this study confirm that paint adherence is better on PP/EP than on PP. Paint debonding is located between the CPO layer and the substrate for both PP and PP/EP plates. AFM and FMM analyses of the substrate side of failure surfaces reveal that paint debonding occurs with plastic deformation only in the EP rubber. Consequently, the increase of adherence with EP introduction in PP could be explained by increased energy dissipation in the elastomer. Moreover, the magnitude of the EP plastic deformation is found to decrease when the depth location of the nodule below the surface increases. This emphasises the important role played by the surface morphology on adhesion properties.

Acknowledgements

E.T. gratefully acknowledges the Belgian Funds for Research in Industry and Agriculture (FRIA) for its financial support. B.N. is Research Associate of the Belgian National Funds for Scientific Research (FNRS).

References

[1] Brewis DM, Briggs D. Polymer 1981;22:7.
[2] Bonnerup C, Gatenholm P. J Adh Sci Technol 1993;7:247.
[3] Clemens RJ, Batts GN, Lawniczak JE, Middleton KP, Sass C. Prog Org Coat 1994;24:43.
[4] Prater TJ, Kaberline SL, Holubka JW, Ryntz RA. J Coat Technol 1996;68:83.
[5] Ryntz RA, Xie Q, Ramamurthy AC. J Coat Technol 1995;67:45.
[6] Ryntz RA, Buzdon B. Prog Org Coat 1971;32:167.
[7] Schmitz PJ, Holubka JW. J Adh 1995;48:137.
[8] Waddington S, Briggs D. Polym Commun 1991;32:506.
[9] Tomasetti E, Daoust D, Bertrand P, Legras R, Rouxhet PG. J Adh Sci Technol 2000 in press.
[10] Maugis D, Barquins M. J Phys D: Appl Phys 1978;11:1989.
[11] Brown HR. IBM J Res Develop 1994;38:379.
[12] Tomasetti E, Nysten B, Legras R. Nanotechnology 1998;9:305.
[13] Tomasetti E, Nysten B, Poleunis C, Bertrand P, Rouxhet PG, Legras R. Surf Interf Anal 1999;27:735.
[14] Gerin PA, Dengis PB, Rouxhet PG. J Chim Phys PCB 1995;92:1043.
[15] Rouxhet PG, Genet MJ. In: Mozes N, Handly PS, Bussher HJ, Rouxhet PG, editors. Microbial cell surface analysis, New York: VCH Publishers, 1991. p. 175–220.
[16] Shirley DA. Phys Rev B 1972;5:4709.
[17] Meyer G, Amer NM. Appl Phys Lett 1990;53:2400.
[18] Maivald P, Butt HJ, Gould SAC, Prater CB, Drake B, Gurley JA, Elings VB, Hansma PK. Nanotechnology 1991;2:103.
[19] Radmacher M, Tillmann RW, Gaub HE. Biophys J 1993;64:735.
[20] Bosma M, Oosterbroek M. Int J Adh Adhesives 1994;14:93.